JOURNAL OF PETROLOGY | VOLUME 46 | NUMBER 8 | PAGES 1645–1659 | 2005 | doi:10.1093/petrology/egi029

Continuous Gradations among Primary Carbonatitic, Kimberlitic, Melilititic, Basaltic, Picritic, and Komatiitic Melts in Equilibrium with Garnet Lherzolite at 3–8 GPa

GUDMUNDUR H. GUDFINNSSON[1]* AND DEAN C. PRESNALL[1,2]

[1]GEOPHYSICAL LABORATORY, CARNEGIE INSTITUTION OF WASHINGTON, 5251 BROAD BRANCH RD, NW, WASHINGTON, DC 20015-1305, USA

[2]DEPARTMENT OF GEOSCIENCES, UNIVERSITY OF TEXAS AT DALLAS, P.O. BOX 830688, RICHARDSON, TX 75083-0688, USA

RECEIVED MAY 28, 2004; ACCEPTED FEBRUARY 17, 2005
ADVANCE ACCESS PUBLICATION MARCH 18, 2005

Multianvil melting experiments in the system CaO–MgO–Al_2O_3–SiO_2–CO_2 (CMAS–CO_2) at 3–8 GPa, 1340–1800°C, involving the garnet lherzolite phase assemblage in equilibrium with CO_2-bearing melts, yield continuous gradations in melt composition between carbonatite, kimberlite, melilitite, komatiite, picrite, and basalt melts. The phase relations encompass a divariant surface in P–T *space. Comparison of the carbonatitic melts produced at the low-temperature side of this surface with naturally occurring carbonatites indicates that natural magnesiocarbonatites could be generated over a wide range of pressures >2·5 GPa. Melts analogous to kimberlites form at higher temperatures along the divariant surface, which suggests that kimberlite genesis requires more elevated geotherms. However, the amount of water found in some kimberlites has the potential to lower temperatures for the generation of kimberlitic melts by up to 150°C, provided no hydrous phases are present. Compositions resembling group IB and IA kimberlites are produced at pressures around 5–6 GPa and 10 GPa, respectively, whereas the compositions of some other kimberlites suggest generation at higher pressures still. At pressures < 4 GPa, an elevated geotherm produces melilitite-like melt in the CMAS–CO_2 system rather than kimberlite. Even when a relatively CO_2-rich mantle composition containing 0·15 wt % CO_2 is assumed, kimberlites and melilitites are produced by <1% melting and carbonatites are generated by even smaller degrees of melting of <0·5%.*

KEY WORDS: *carbonatite; CO_2; kimberlite; melilitite; melt generation*

INTRODUCTION

On the scale of global volcanic activity, the amounts of kimberlites and carbonatites are minute, but they have provided a great amount of information about the state of the interior of the Earth. A number of models have been proposed for the generation of carbonatite (Bailey, 1993, and references therein) and kimberlite magmas (Mitchell, 1995, and references therein), and the presence of CO_2 plays a key role in these models. It has also been argued that small amounts of CO_2, which lower the solidus of peridotite and lead to incipient melting, are the cause of the seismic low-velocity zone (Wyllie & Huang, 1975; Eggler, 1976; Presnall & Gudfinnsson, 2005). Additionally, CO_2-rich carbonatitic and kimberlitic melts may influence the trace element chemistry of mid-ocean ridge basalts (MORB) (Presnall *et al.*, 2002) and cause reduced seismic velocities in parts of the upper and lower mantle (Presnall & Gudfinnsson, 2005). Determination of the melting behavior of carbonated lherzolite is, therefore, of great interest.

Geochemical evidence suggests that at least some kimberlite (Smith *et al.*, 1985) and carbonatite magmas (Nelson *et al.*, 1988; Harmer & Gittins, 1998) are derived by partial melting of the asthenospheric mantle. Because of the high concentrations of incompatible trace elements in carbonatites and kimberlites, their generation by very small degrees of melting is inferred (Nelson *et al.*, 1988).

*Corresponding author. Fax: (202) 478 8901.
E-mail: g.gudfinnsson@gl.ciw.edu

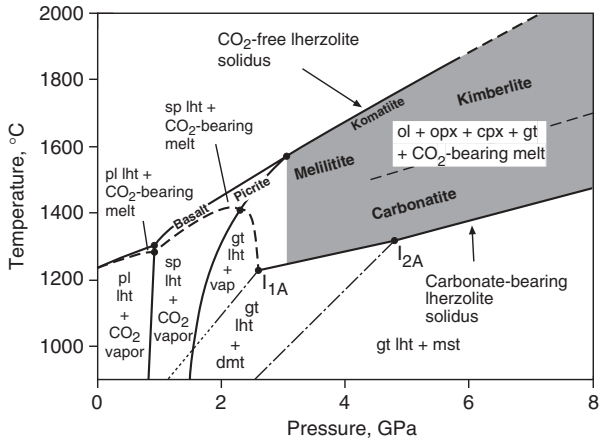

Fig. 1. Pressure–temperature diagram showing the solidus of plagioclase, spinel and garnet lherzolite in the CMAS–CO_2 system under CO_2-free and CO_2-bearing conditions. The divariant region between the CO_2-bearing (carbonate-bearing above 2·6 GPa) and CO_2-free solidi is divided into three different areas: an area where CO_2-bearing melt coexists with (1) plagioclase lherzolite phase assemblage, (2) spinel lherzolite phase assemblage, and (3) garnet lherzolite phase assemblage (ol + opx + cpx + gt). The data presented here are from this last area in the 3–8 GPa pressure range (shaded). The points on the CO_2-bearing solidus curve at about 2·6 and 4·8 GPa (marked I_{1A} and I_{2A}; Dalton & Presnall, 1998*a*) denote the transitions on the solidus from CO_2 vapor-bearing to dolomite-bearing garnet lherzolite and dolomite-bearing to magnesite-bearing garnet lherzolite, respectively. The subsolidus univariant lines emanating from these points are also shown. The intersection of the spinel lherzolite to garnet lherzolite transition with the subsolidus univariant line extending from invariant point I_{1A} is uncertain. The dashed line on the divariant surface indicates the approximate division in the system between carbonatitic melts, on the one hand, and kimberlitic and melilititic melts, on the other. ol, olivine; opx, orthopyroxene; cpx, clinopyroxene; gt, garnet; dmt, dolomite; mst, magnesite; pl, plagioclase; sp, spinel; vap, CO_2 vapor; lht, lherzolite. Modified after Dalton & Presnall (1998*a*) and Presnall *et al.* (2002).

Experiments to determine the phase equilibria relevant to incipient melting of upper mantle peridotite are technically difficult. As a consequence of the small amount of melt present, it is hard to maintain equilibrium during the experiments. Additionally, the melts generated are almost invariably modified upon quenching and impossible to analyze because of their very small volume. However, by reducing the number of components, and hence the variance of the system, the task becomes reasonable in scope.

The system CaO–MgO–Al_2O_3–SiO_2–CO_2 (CMAS–CO_2) is a realistic model system to investigate phase equilibria involving mantle peridotite in equilibrium with CO_2-bearing melts (Dalton & Presnall, 1998*a*, 1998*b*). The garnet lherzolite phase assemblage of olivine, orthopyroxene, clinopyroxene, and garnet coexists with melt along a divariant surface in P–T space in the five-component CMAS–CO_2 system (Fig. 1). On the low-temperature side, the divariant surface is bounded by a univariant solidus curve, along which the garnet lherzolite phase assemblage is joined by dolomite or magnesite. On the high-temperature side, the CO_2-free garnet lherzolite solidus delimits the surface. As the P–T slope of the CO_2-free solidus is considerably greater than that of the carbonate-bearing solidus, the temperature difference between these curves increases with pressure. At a fixed pressure and temperature, the garnet lherzolite plus liquid phase assemblage is invariant and the compositions of all phases are uniquely defined, independent of the bulk composition of the system. This means that a starting composition can be chosen so as to maximize the amount of any phase. In our case, the starting compositions were designed to yield experiments with large amount of melt present. Once the phase equilibrium data have been acquired, algebraic methods allow calculation of melting paths for any arbitrary mantle composition in the CMAS–CO_2 system (Presnall, 1986), including melting paths where very small amounts of liquid are present.

A link between carbonatite and kimberlite magmas was suggested a long time ago and many researchers have since argued for a relationship between these two kinds of magma (e.g. Barker, 1989; Bailey, 1993). The nature of this relationship is controversial, however. In earlier experiments in the CMAS–CO_2 system, Dalton & Presnall (1998*a*, 1998*b*) determined the carbonate-bearing solidus at 3–7 GPa (Dalton & Presnall, 1998*a*) and the 6 GPa isobar (Dalton & Presnall, 1998*b*) on the divariant surface with garnet lherzolite in equilibrium with CO_2-bearing melt. They concluded that both carbonatitic and kimberlitic magmas could be generated by melting of CO_2-bearing garnet lherzolite but at different temperatures and degrees of melting. According to this model, kimberlites and carbonatites are related by a similar source rather than by fractionation or liquid immiscibility, and there is gradational change between the two kinds of melts. In this paper, we expand the results presented by Dalton & Presnall (1998*a*, 1998*b*) to include a determination of melting relations throughout the P–T region bounded by the 3 and 8 GPa isobars and the two solidus curves (Fig. 1). This provides a fuller picture of how melt compositions change with P and T. Our experimental data confirm the continuous gradations between carbonatites, kimberlites, and komatiites observed by Dalton & Presnall (1998*b*); however, in addition, we note the gradation of kimberlite compositions toward melilitite compositions at the low-pressure end of the data array and toward basaltic and picritic compositions close to the CO_2-free lherzolite solidus at pressures below about 4 GPa, not explored by Dalton & Presnall.

METHODS

The melting experiments were conducted at the Geophysical Laboratory using a multianvil apparatus.

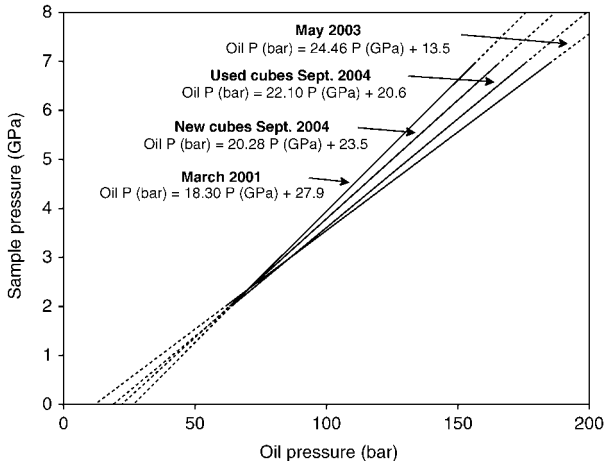

Fig. 2. Pressure calibrations of the 18/11 multianvil assemblies at the Geophysical Laboratory. All the calibration lines are constrained by bracketing the quartz–coesite transition at 3·22 GPa, 1200°C and the garnet–perovskite transition of $CaGeO_3$ at 5·99 GPa, 1140°C. All the experiments were conducted with identical assemblies and with the same multianvil apparatus. The calibrations from March 2001 and May 2003 were carried out with the same set of tungsten carbide anvils. Two comparison calibrations were performed in September 2004 with, on the one hand, a previously unused set of anvils and, on the other, a used set. The calibrations clearly show a decrease in pressure efficiency of the tungsten carbide anvils with use. The difference in the calibration lines at the quartz–coesite transition at 3·22 GPa is small but the difference increases with pressure. In determining the sample pressure in the experiments presented in Tables 2 and 3, we assume a linear change between the calibrations from March 2001 and May 2003.

For pressure calibration, we used the transition of quartz to coesite at 3·22 GPa, 1200°C (Bohlen & Boettcher, 1982) and the transition of $CaGeO_3$ from garnet to perovskite structure at 5·99 GPa, 1140°C (Susaki *et al.*, 1985). We noticed changes in the pressure calibration with time (Fig. 2) that appear to be related to a permanent deformation of the tungsten carbide anvils that were used in the experiments. This can be seen from the fact that the truncated corners of the cubes became slightly concave with increasing use. To determine sample pressures, we have corrected for these changes. Methods for preparing starting mixtures, experimental procedures, and treatment of run products have been described in detail by Dalton & Presnall (1998*b*). Briefly, each starting mixture is composed of a mixture of a silicate glass and natural magnesite powder. All the starting mixtures (Table 1) except one (CMASCO2-1), were prepared by Dalton & Presnall (1998*a*, 1998*b*). Welding of the sample capsules usually causes some loss of CO_2, and hence the CO_2 contents reported in Table 1 are the maximum possible amounts. Whenever possible, the experiments ran for 6 h, but because many of the experiments were at pressures and temperatures within the stability field of diamond, the graphite heaters used in the run assemblies gradually became unstable. As a consequence, some of the runs are

Table 1: Composition of starting mixtures in wt %

Starting mixture	CaO	MgO	Al_2O_3	SiO_2	CO_2*
JADSCM-3	21·36	25·68	3·04	27·54	22·82
JADSCM-7	10·95	33·38	4·02	43·15	8·50
JADSCM-8	12·48	32·76	3·31	39·21	12·24
JADSCM-14	9·74	34·20	4·90	46·57	4·59
CMASCO2-1	11·24	31·96	6·39	45·41	5·00

*The amount of CO_2 in the starting mixtures as prepared. Some CO_2 was usually lost when the sample capsules were welded.

shorter than 6 h (Table 2). The experimental conditions and the resulting phase assemblages are listed in Table 2. During preparation of polished sections special care was taken to prevent CO_2 loss by not exposing the samples to water at any stage, and the samples were repeatedly impregnated with epoxy under vacuum to reduce plucking. All the crystalline phases and quenched melts were analyzed using a JEOL JXA-8800 electron microprobe at the Geophysical Laboratory, with an accelerating voltage of 15 kV, a rastering beam covering an area <5–15 μm on each side and a 15 nA probe current. Crystalline diopside (DJ35) was used as a standard. When possible, at least 10 analyses of the crystalline phases were acquired, but because of their small size (usually <5 μm diameter), as few as three analyses of garnet had to suffice. In almost all of the experiments, except for the very few exceptions when glass formed, melt became an intergrowth of silicate and carbonate phases on quenching, sometimes very coarse (Fig. 3). Because of this, it was usually more difficult to obtain good analyses of the melt phase than the crystalline phases, which is reflected in the standard deviations of the oxides (Table 3). In some cases, the roughness of the quenched melts limited the number of analyses that could be safely acquired, but in other cases the quenched melts were homogeneous and smooth enough to allow relatively few analyses. Correspondingly, from 12 to 70 points were analyzed in the areas of quenched melt. Analyses were reduced using the ZAF correction routine and the amount of CO_2 in melts and magnesite was calculated by difference. In calculating the matrix corrections for melts and magnesite, the program assumes that the oxide not being analyzed is CO_2, which leads to small differences, mainly lower CO_2 and higher MgO contents, relative to not considering the effect of CO_2 on the properties of the matrix. The compositions of the coexisting melts and crystalline phases are reported in Table 3. Two experiments at 5 GPa at the CO_2-free solidus and at the carbonate-bearing solidus (Fig. 1) reproduce the results of Weng (1997) and Dalton & Presnall (1998*a*), respectively,

Table 2: Experimental conditions and resulting phase assemblages

Run no.	Starting mixture	Pressure (GPa)	Temperature (°C)	Duration (h)	Phase assemblage
PR-126	JADSCM-7	3·2	1400	6	ol + opx + cpx + gt + liq
PR-121	JADSCM-7	3·2	1450	6	ol + opx + cpx + gt + liq
PR-120	CMASCO2-1	3·2	1550	4	ol + opx + cpx + gt + liq
PR-97	CMASCO2-1	3·3	1510	6	ol + opx + cpx + gt + liq
PR-92	JADSCM-7	3·7	1450	6	ol + opx + cpx + gt + liq
PR-91	CMASCO2-1	3·7	1550	6	ol + opx + cpx + gt + liq
PR-53	JADSCM-7	3·9	1500	6	ol + opx + cpx + gt + liq
PR-66	JADSCM-14	4·7	1650	4	ol + opx + cpx + gt + liq
PR-46	JADSCM-8	4·9	1400	6	ol + opx + cpx + gt + liq
PR-31	JADSCM-7	4·9	1480	6	ol + opx + cpx + gt + liq
PR-39	JADSCM-7	4·9	1530	6	ol + opx + cpx + gt + liq
PR-22	JADSCM-3	5·0	1340	6·1	ol + opx + cpx + gt + mst + liq
PR-28	JADSCM-8	5·9	1455	6	ol + opx + cpx + gt + liq
PR-72	JADSCM-14	6·5	1800	3	ol + opx + cpx + gt + liq
PR-60	JADSCM-14	6·7	1750	3	ol + opx + cpx + gt + liq
PR-52	JADSCM-7	6·8	1650	6	ol + opx + cpx + gt + liq
PR-106	JADSCM-8	6·9	1460	6	ol + opx + cpx + gt + (mst) + liq
PR-35	JADSCM-8	6·9	1550	6	ol + opx + cpx + gt + liq
PR-90	JADSCM-8	7·1	1500	6	ol + opx + cpx + gt + liq
PR-55	JADSCM-7	7·6	1700	3	ol + opx + cpx + gt + liq
PR-40	JADSCM-8	7·8	1550	6	ol + opx + cpx + gt + liq
PR-131	JADSCM-7	8·0	1800	0·33	ol + opx + cpx + gt + liq

ol, olivine; opx, orthopyroxene; cpx, clinopyroxene; gt, garnet; mst, magnesite; liq, liquid. Parentheses indicate disequilibrium phase.

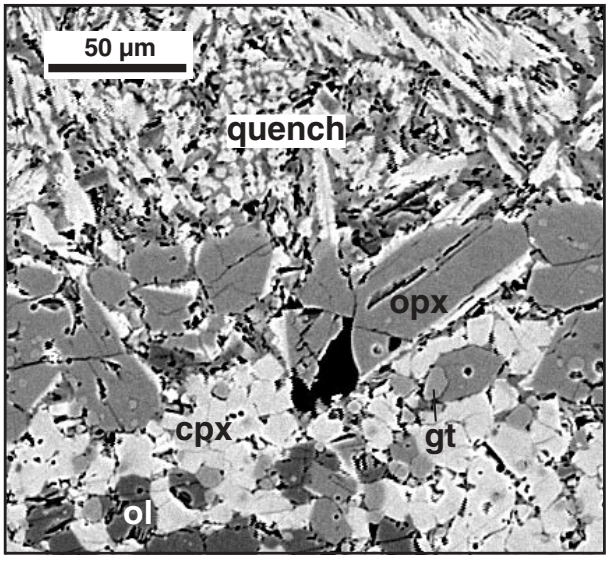

Fig. 3. Backscattered electron image of run PR-60 (6·7 GPa, 1750°C). The quench area at the top is composed of a coarse intergrowth of a silicate phase (light) and a carbonate phase (dark). ol, olivine; opx, orthopyroxene; cpx, clinopyroxene; gt, garnet.

very well with the amounts of all of the oxides in the melts differing by less than the one standard deviation uncertainty.

No reversal experiments have been conducted in this study and attainment of chemical equilibrium has not been proved. Earlier works in CO_2-rich systems at high temperatures and high pressures (e.g. Irving & Wyllie, 1975) have indicated very fast equilibration rates, requiring experiments as short as <1 h to reach equilibrium. The lack of zoning in our crystalline run products is also consistent with near-equilibrium conditions. For further discussion on attainment of equilibrium, we refer to the paper of Dalton & Presnall (1998*a*), as the assemblies and procedures were essentially the same in the two studies.

MELT COMPOSITIONS

None of our experimental run products show signs of liquid immiscibility and there are continuous gradations between all the melt compositions reported here. On the high-pressure side of the divariant surface containing melts in equilibrium with garnet lherzolite in the

Table 3: Electron microprobe analyses of crystalline phases and quenched melts (wt %)

Experiment	CaO	MgO	Al_2O_3	SiO_2	CO_2*	Total
PR-126 (3·2 GPa/1400°C)						
Olivine (9)†	0·33 (0·05)‡	57·25 (0·38)	0·11 (0·06)	42·10 (0·33)		99·79 (0·21)
Opx (10)	2·32 (0·09)	36·98 (0·42)	4·33 (0·48)	55·85 (0·40)		99·48 (0·19)
Cpx (9)	19·28 (0·30)	22·86 (0·36)	3·78 (0·22)	54·02 (0·44)		99·94 (0·45)
Garnet (6)	7·22 (0·74)	25·60 (0·49)	23·00 (1·27)	44·88 (0·68)		100·70 (0·27)
Quench (25)	31·52 (2·21)	19·70 (2·15)	0·67 (0·29)	7·87 (2·54)	40·24 (2·32)	
PR-121 (3·2 GPa/1450°C)						
Olivine (10)	0·27 (0·02)	57·37 (0·31)	0·09 (0·02)	42·02 (0·25)		99·75 (0·45)
Opx (12)	2·46 (0·17)	36·51 (0·20)	4·70 (0·22)	56·09 (0·33)		99·75 (0·46)
Cpx (11)	18·15 (0·55)	23·81 (0·57)	3·66 (0·59)	53·90 (0·63)		99·53 (0·40)
Garnet (8)	6·08 (0·33)	25·81 (0·53)	23·86 (0·87)	44·43 (0·46)		100·18 (0·32)
Quench (30)	31·69 (0·48)	19·24 (0·35)	0·86 (0·06)	9·45 (0·70)	38·75 (0·65)	
PR-120 (3·2 GPa/1550°C)						
Olivine (10)	0·36 (0·06)	57·16 (0·17)	0·14 (0·03)	42·50 (0·18)		100·16 (0·10)
Opx (12)	2·63 (0·07)	36·06 (0·22)	5·13 (0·39)	55·87 (0·33)		99·69 (0·20)
Cpx (12)	15·18 (0·31)	25·46 (0·28)	5·12 (0·29)	53·81 (0·39)		99·56 (0·32)
Garnet (12)	5·69 (0·19)	25·79 (0·12)	24·45 (0·27)	44·08 (0·14)		100·01 (0·18)
Quench (18)	19·43 (0·28)	23·60 (0·30)	6·42 (0·11)	35·28 (0·50)	15·26 (0·83)	
PR-97 (3·3 GPa/1510°C)						
Olivine (12)	0·31 (0·04)	57·47 (0·18)	0·15 (0·05)	42·62 (0·19)		100·56 (0·24)
Opx (15)	2·59 (0·14)	35·70 (0·34)	5·88 (0·49)	56·11 (0·37)		100·27 (0·32)
Cpx (15)	16·32 (0·44)	24·19 (0·45)	6·42 (0·47)	53·32 (0·35)		100·25 (0·30)
Garnet (12)	6·16 (0·22)	25·24 (0·15)	24·46 (0·25)	44·20 (0·28)		100·05 (0·35)
Quench (12)	19·48 (0·32)	22·99 (0·21)	7·68 (0·15)	35·63 (0·67)	14·21 (0·65)	
PR-92 (3·7 GPa/1450°C)						
Olivine (7)	0·39 (0·12)	57·81 (0·33)	0·15 (0·07)	42·54 (0·26)		100·89 (0·08)
Opx (14)	2·47 (0·21)	36·73 (0·20)	5·15 (0·37)	56·35 (0·30)		100·70 (0·25)
Cpx (11)	17·85 (0·52)	23·70 (0·39)	4·48 (0·37)	54·13 (0·52)		100·16 (0·31)
Garnet (10)	6·08 (0·27)	26·62 (0·32)	23·85 (0·96)	44·69 (0·54)		101·24 (0·17)
Quench (42)	31·66 (2·10)	19·52 (1·62)	1·56 (0·53)	12·83 (3·57)	34·43 (3·15)	
PR-91 (3·7 GPa/1550°C)						
Olivine (11)	0·27 (0·03)	58·21 (0·15)	0·11 (0·02)	42·30 (0·17)		100·89 (0·16)
Opx (13)	2·57 (0·07)	36·81 (0·29)	4·84 (0·38)	56·61 (0·27)		100·83 (0·26)
Cpx (20)	16·13 (0·65)	25·14 (0·52)	4·83 (0·38)	54·33 (0·37)		100·43 (0·33)
Garnet (12)	5·77 (0·18)	26·48 (0·19)	24·73 (0·24)	44·17 (0·23)		101·15 (0·27)
Quench (27)	19·94 (0·17)	24·64 (0·17)	6·74 (0·08)	36·08 (0·43)	12·59 (0·72)	
PR-53 (3·9 GPa/1500°C)						
Olivine (10)	0·22 (0·02)	58·04 (0·12)	0·08 (0·01)	42·44 (0·18)		100·77 (0·19)
Opx (11)	2·64 (0·13)	36·98 (0·42)	3·94 (0·97)	57·14 (0·68)		100·70 (0·14)
Cpx (12)	18·02 (0·40)	23·78 (0·47)	4·27 (0·32)	54·38 (0·30)		100·45 (0·29)
Garnet (8)	6·23 (0·13)	25·52 (0·06)	24·92 (0·12)	44·23 (0·22)		100·90 (0·22)
Quench (50)	25·70 (1·40)	22·16 (1·39)	2·57 (0·29)	21·73 (2·09)	27·85 (1·77)	
PR-66 (4·7 GPa/1650°C)						
Olivine (12)	0·29 (0·01)	57·70 (0·16)	0·14 (0·01)	42·77 (0·10)		100·89 (0·15)
Opx (12)	2·78 (0·04)	37·03 (0·11)	3·43 (0·14)	57·74 (0·17)		100·98 (0·12)
Cpx (11)	13·28 (0·30)	27·90 (0·26)	3·31 (0·12)	55·85 (0·16)		100·33 (0·21)

Table 3: continued

Experiment	CaO	MgO	Al_2O_3	SiO_2	CO_2*	Total
Garnet (10)	5·16 (0·09)	26·54 (0·23)	24·76 (0·22)	44·78 (0·14)		101·23 (0·17)
Quench (51)	15·17 (1·84)	27·83 (1·82)	6·43 (0·98)	40·82 (5·68)	9·74 (4·40)	
PR-46 (4·9 GPa/1400°C)						
Olivine (6)	0·34 (0·11)	57·08 (0·49)	0·09 (0·06)	42·94 (0·25)		100·45 (0·32)
Opx (11)	2·32 (0·23)	37·89 (0·22)	1·77 (0·11)	58·41 (0·39)		100·38 (0·33)
Cpx (10)	19·68 (0·46)	23·58 (0·49)	1·45 (0·18)	55·54 (0·71)		100·24 (0·44)
Garnet (4)	5·89 (0·22)	26·36 (0·34)	22·77 (0·93)	44·85 (0·54)		99·87 (0·26)
Quench (23)	31·23 (1·48)	21·22 (2·17)	0·38 (0·19)	6·37 (2·76)	40·79 (3·13)	
PR-31 (4·9 GPa/1480°C)						
Olivine (10)	0·29 (0·06)	57·45 (0·37)	0·08 (0·03)	41·61 (0·23)		99·42 (0·37)
Opx (10)	2·46 (0·12)	37·76 (0·26)	2·26 (0·23)	57·58 (0·61)		100·06 (0·71)
Cpx (10)	18·22 (0·33)	24·69 (0·41)	1·98 (0·10)	55·03 (0·33)		99·92 (0·43)
Garnet (9)	5·73 (0·31)	26·67 (0·25)	23·93 (0·63)	43·85 (0·47)		100·18 (0·40)
Quench (60)	27·14 (1·32)	23·47 (2·17)	1·21 (0·43)	14·64 (2·96)	33·54 (2·47)	
PR-39 (4·9 GPa/1530°C)						
Olivine (10)	0·30 (0·09)	57·71 (0·20)	0·08 (0·01)	41·85 (0·27)		99·93 (0·30)
Opx (9)	2·29 (0·28)	37·86 (0·32)	2·09 (0·27)	57·64 (0·46)		99·89 (0·58)
Cpx (10)	17·75 (0·58)	24·82 (0·39)	1·94 (0·08)	55·21 (0·52)		99·72 (0·56)
Garnet (10)	5·84 (0·47)	26·57 (0·34)	23·92 (0·59)	43·81 (0·63)		100·14 (0·74)
Quench (68)	25·03 (1·69)	24·16 (3·34)	1·76 (0·53)	19·32 (3·58)	29·73 (2·83)	
PR-22 (5·0 GPa/1340°C)						
Olivine (9)	0·27 (0·09)	58·04 (0·23)	0·04 (0·02)	42·96 (0·13)		101·31 (0·30)
Opx (11)	2·00 (0·15)	38·35 (0·15)	1·52 (0·18)	59·39 (0·40)		101·26 (0·46)
Cpx (10)	22·32 (1·09)	21·22 (1·23)	1·86 (0·73)	55·15 (0·43)		100·15 (0·37)
Garnet (10)	7·16 (0·83)	25·54 (0·91)	23·55 (1·03)	43·84 (0·84)		100·08 (0·92)
Magnesite (9)	9·53 (0·46)	41·60 (0·41)	0·01 (0·01)	0·04 (0·04)	48·82 (0·24)	
Quench (20)	30·46 (1·86)	22·63 (2·46)	0·73 (0·85)	4·75 (2·01)	41·43 (2·49)	
PR-28 (5·9 GPa/1455°C)						
Olivine (10)	0·18 (0·02)	57·79 (0·26)	0·05 (0·02)	42·99 (0·26)		101·00 (0·26)
Opx (10)	2·10 (0·16)	38·10 (0·30)	1·41 (0·14)	59·56 (0·15)		101·18 (0·27)
Cpx (10)	20·11 (0·31)	23·05 (0·24)	1·19 (0·12)	56·49 (0·43)		100·83 (0·47)
Garnet (11)	5·34 (0·20)	25·98 (0·15)	24·20 (0·28)	45·25 (0·28)		100·77 (0·51)
Quench (60)	26·32 (1·48)	24·73 (3·21)	0·78 (0·30)	13·66 (3·32)	34·51 (2·13)	
PR-72 (6·5 GPa/1800°C)						
Olivine (10)	0·27 (0·01)	57·74 (0·16)	0·16 (0·02)	42·71 (0·10)		100·86 (0·15)
Opx (12)	2·82 (0·05)	37·40 (0·08)	2·41 (0·16)	58·59 (0·17)		101·22 (0·12)
Cpx (12)	11·12 (0·45)	30·27 (0·42)	2·30 (0·13)	57·10 (0·08)		100·78 (0·16)
Garnet (8)	4·54 (0·07)	27·64 (0·11)	23·82 (0·08)	45·42 (0·10)		101·42 (0·09)
Quench (48)	14·91 (1·33)	28·01 (1·76)	5·33 (0·64)	43·38 (4·58)	8·37 (3·30)	
PR-60 (6·7 GPa/1750°C)						
Olivine (13)	0·27 (0·02)	57·20 (0·19)	0·12 (0·02)	41·48 (0·31)		99·07 (0·24)
Opx (11)	2·79 (0·09)	37·28 (0·31)	1·97 (0·09)	57·13 (0·30)		99·17 (0·26)
Cpx (10)	12·93 (1·02)	28·73 (0·83)	2·00 (0·15)	55·36 (0·20)		99·02 (0·17)
Garnet (10)	4·68 (0·08)	26·77 (0·14)	24·12 (0·10)	44·20 (0·39)		99·77 (0·31)
Quench (50)	17·36 (1·93)	27·74 (2·05)	3·99 (0·59)	37·68 (5·65)	13·23 (4·63)	

Experiment	CaO	MgO	Al_2O_3	SiO_2	CO_2*	Total
PR-52 (6·8 GPa/1650° C)						
Olivine (11)	0·24 (0·04)	58·13 (0·18)	0·08 (0·03)	42·74 (0·09)		101·18 (0·17)
Opx (11)	2·63 (0·13)	38·15 (0·13)	1·73 (0·24)	58·59 (0·22)		101·10 (0·16)
Cpx (10)	15·26 (0·93)	27·35 (0·76)	1·56 (0·13)	56·60 (0·24)		100·78 (0·10)
Garnet (10)	4·87 (0·07)	27·17 (0·13)	24·36 (0·18)	45·09 (0·08)		101·49 (0·29)
Quench (75)	24·80 (1·45)	26·99 (1·45)	1·70 (0·44)	23·02 (5·40)	23·50 (4·49)	
PR-106 (6·9 GPa/1460° C)						
Olivine (6)	0·24 (0·05)	58·09 (0·13)	0·06 (0·02)	43·16 (0·13)		101·55 (0·16)
Opx (6)	1·88 (0·13)	38·73 (0·17)	1·04 (0·21)	59·21 (0·17)		100·86 (0·16)
Cpx (10)	20·07 (0·39)	23·54 (0·31)	0·93 (0·17)	55·88 (0·41)		100·42 (0·41)
Garnet (6)	5·42 (0·47)	27·32 (0·61)	23·28 (0·78)	44·80 (0·70)		100·82 (0·81)
Quench (25)	27·19 (3·10)	25·00 (4·29)	0·29 (0·20)	8·48 (4·80)	39·03 (4·73)	
PR-35 (6·9 GPa/1550° C)						
Olivine (10)	0·30 (0·11)	57·43 (0·61)	0·12 (0·10)	42·36 (0·60)		100·21 (0·31)
Opx (11)	2·34 (0·30)	37·96 (0·41)	1·35 (0·20)	57·99 (0·35)		99·63 (0·35)
Cpx (10)	17·61 (0·21)	25·10 (0·21)	1·28 (0·25)	55·31 (0·31)		99·30 (0·26)
Garnet (9)	5·44 (0·28)	27·12 (0·21)	23·57 (0·47)	43·62 (0·44)		99·76 (0·61)
Quench (50)	25·18 (1·98)	25·43 (2·06)	0·89 (0·35)	15·70 (5·30)	32·80 (4·13)	
PR-90 (7·1 GPa/1500° C)						
Olivine (8)	0·19 (0·05)	58·48 (0·14)	0·03 (0·01)	45·52 (0·14)		101·22 (0·11)
Opx (11)	2·30 (0·36)	38·57 (0·39)	1·54 (0·52)	58·73 (0·50)		101·14 (0·23)
Cpx (13)	18·47 (0·50)	24·84 (0·42)	1·04 (0·08)	56·32 (0·45)		100·67 (0·38)
Garnet (4)	5·30 (0·08)	26·98 (0·08)	24·00 (0·25)	44·82 (0·20)		101·09 (0·40)
Quench (50)	27·40 (1·22)	23·81 (2·11)	0·64 (0·25)	12·12 (2·76)	36·04 (2·38)	
PR-55 (7·6 GPa/1700° C)						
Olivine (7)	0·26 (0·02)	57·71 (0·21)	0·11 (0·04)	42·65 (0·14)		100·73 (0·25)
Opx (9)	2·66 (0·09)	37·95 (0·14)	1·80 (0·24)	58·50 (0·19)		100·91 (0·09)
Cpx (10)	14·01 (0·19)	28·46 (0·19)	1·65 (0·10)	56·61 (0·14)		100·73 (0·18)
Garnet (10)	4·88 (0·25)	27·18 (0·36)	24·18 (0·15)	45·09 (0·27)		101·33 (0·35)
Quench (40)	19·69 (3·15)	29·08 (2·59)	2·21 (1·21)	28·46 (12·65)	20·56 (10·57)	
PR-40 (7·8 GPa/1550° C)						
Olivine (10)	0·24 (0·06)	57·58 (0·08)	0·07 (0·03)	42·16 (0·21)		100·05 (0·20)
Opx (8)	2·54 (0·45)	37·54 (0·50)	1·89 (0·55)	57·62 (0·66)		99·58 (0·44)
Cpx (9)	18·19 (0·27)	24·93 (0·29)	0·98 (0·14)	55·60 (0·41)		99·70 (0·38)
Garnet (6)	5·17 (0·23)	27·38 (0·24)	23·00 (0·43)	44·70 (0·47)		100·24 (0·39)
Quench (50)	22·10 (1·45)	27·51 (2·54)	0·89 (0·28)	17·04 (2·41)	32·45 (2·10)	
PR-131 (8·0 GPa/1800° C)						
Olivine (6)	0·23 (0·01)	58·73 (0·23)	0·09 (0·00)	41·48 (0·32)		100·53 (0·43)
Opx (8)	2·58 (0·22)	38·08 (0·30)	1·89 (0·50)	57·29 (0·57)		99·84 (0·50)
Cpx (4)	11·42 (0·16)	30·56 (0·25)	1·29 (0·17)	56·20 (0·91)		99·47 (0·83)
Garnet (2)	4·48 (0·08)	28·18 (0·13)	22·61 (0·60)	45·29 (1·50)		100·55 (0·95)
Quench (36)	16·82 (3·12)	30·40 (4·66)	2·45 (0·98)	32·06 (10·95)	18·28 (9·49)	

*The amount of CO_2 is calculated by difference. Further explanation is given in the text. The 1σ uncertainty for CO_2 is based on this amount.
†Number of analyses.
‡Number in parentheses is 1σ analytical uncertainty.

CMAS–CO_2 system, the compositions of melts change continuously from relatively silica-rich (about 47 to >52 wt % SiO_2) komatiitic melts on the CO_2-free solidus (Weng, 1997; J. A. Dalton, unpublished data, 2004) through kimberlitic compositions and, finally, carbonatitic compositions with decreasing temperature (Fig. 1). Dalton & Presnall (1998*b*) reported similar changes along the 6 GPa isobar. Their data are, however, systematically shifted in P–T space relative to the data reported here. The reason for these differences at 6 GPa, which are larger than the 2σ uncertainties of the two datasets, is thus far unknown, but problems with pressure calibration are among the possible explanations. As the trends of the melt and mineral compositions reported here agree well with the carbonate-bearing (Dalton & Presnall, 1998*a*) and CO_2-free (Gudfinnsson & Presnall, 1996; Weng, 1997; Milholland & Presnall, 1998; J. A. Dalton, unpublished data, 2004) solidi (Fig. 1), determined independently in earlier experiments, we feel confident of our data. In Fig. 1, the division between carbonatites and kimberlites is placed where the amount of CO_2 in the liquid translates to about 50% modal carbonate, which is the minimum amount in carbonatites as proposed by Woolley *et al.* (1996). At low pressures, the melts on the carbonate-bearing solidus are also carbonatitic, but with rising temperature the melts become significantly more aluminous and less magnesian than at higher pressures, and at about 3 GPa the melts are more akin to melilitites than kimberlites. Brey & Green (1977) and Brey (1978) proposed the generation of primary melilitite magmas at similar pressures. At even higher temperatures and lower CO_2 contents, the melt composition changes from melilititic to picritic basalt (Gudfinnsson & Presnall, 1996; Milholland & Presnall, 1998).

Figure 4 shows isopleths for all the oxides in the melt. At pressures above 5 GPa, the concentrations of all oxides change nearly linearly with temperature, whereas at lower pressures the contours are not evenly spaced. This is especially apparent on the CaO, Al_2O_3, SiO_2, and CO_2 diagrams. Specifically, on the low-temperature side of the divariant surface at pressures lower that 5 GPa, the composition of the melt does not change much with temperature. Then there is a rapid change in the composition over a small temperature interval, followed by a smaller compositional gradient next to the CO_2-free solidus. This behavior is in excellent agreement with changes in melt composition observed by Moore & Wood (1998) in melting experiments on carbonated lherzolite in the system CaO–MgO–SiO_2–CO_2 at 3 GPa. The curvature of the contours in Fig. 4 at pressures less than 5 GPa may be influenced by the large drop in the solidus temperature of CO_2-bearing lherzolite between 2 and 3 GPa where the stable CO_2-bearing phase at the solidus changes from vapor to carbonate, the so-called 'ledge' (Fig. 1). Moore & Wood (1998) offered this rapid change from carbonatitic melt compositions to silicate melt compositions as a possible explanation for the frequent association of carbonatites and nephelinites–melilitites and the rarity of intermediate compositions. Extrapolation of the isopleths to even lower pressures is not shown because of a lack of data. The curvature in the isopleths indicates that, at pressures just above the ledge, the carbonatite field abruptly expands over a large temperature range at the expense of silicate melts. The melts in this part of the divariant surface have relatively high CaO/MgO.

Figure 5 depicts how the melt compositions change with MgO/CaO and SiO_2/Al_2O_3. This diagram was used by Rock (1991) to distinguish between kimberlites and ultramafic lamprophyres, but it is useful for our purposes because it includes four of the five components in the CMAS–CO_2 system and the amount of the fifth (CO_2) can easily be inferred. One can see that the melt compositions partly extend into the kimberlite field with increasing pressure and temperature. However, melts generated near the carbonated solidus do not become kimberlitic at any pressure in the range of our experiments. As the CO_2 content of melts along the carbonate-bearing solidus changes very little with pressure, this feature is not likely to change for a large range of pressure higher than in our experiments, provided the phase assemblage remains the same.

Carbonatites

At carbonate saturation, the melts coexisting with garnet lherzolite contain 40–45 wt % CO_2, and only 5–6 wt % SiO_2 and <1 wt % Al_2O_3 (Dalton & Presnall, 1998*a*). Hence, the compositions of the carbonatitic melts generated at the carbonate-bearing solidus are essentially those of a carbonate with minor amounts of SiO_2 and Al_2O_3. With rising temperature above the solidus, the amounts of SiO_2 and Al_2O_3 steadily increase at the expense of CaO and CO_2. Carbonatite melts in the CMAS–CO_2 system have $CaO/(CaO + MgO) = 0{\cdot}5$–$0{\cdot}7$, a range similar to the $CaO/(CaO + MgO + FeO + Fe_2O_3 + MnO)$ ratios of natural magnesiocarbonatites and ferrocarbonatites (Woolley & Kempe, 1989) (Fig. 6). The Sarfartoq carbonatites from west Greenland (L. M. Larsen, unpublished data, 2003) plot mostly near the low-pressure end of the carbonate-bearing solidus (Fig. 5). As noted by Dalton & Presnall (1998*b*), the large range in the composition of carbonatites is not surprising considering that they are whole-rock compositions, and thus do not necessarily represent primary liquid compositions.

Kimberlites

Melts analogous to kimberlites are generated at more elevated temperatures than carbonatites and hence

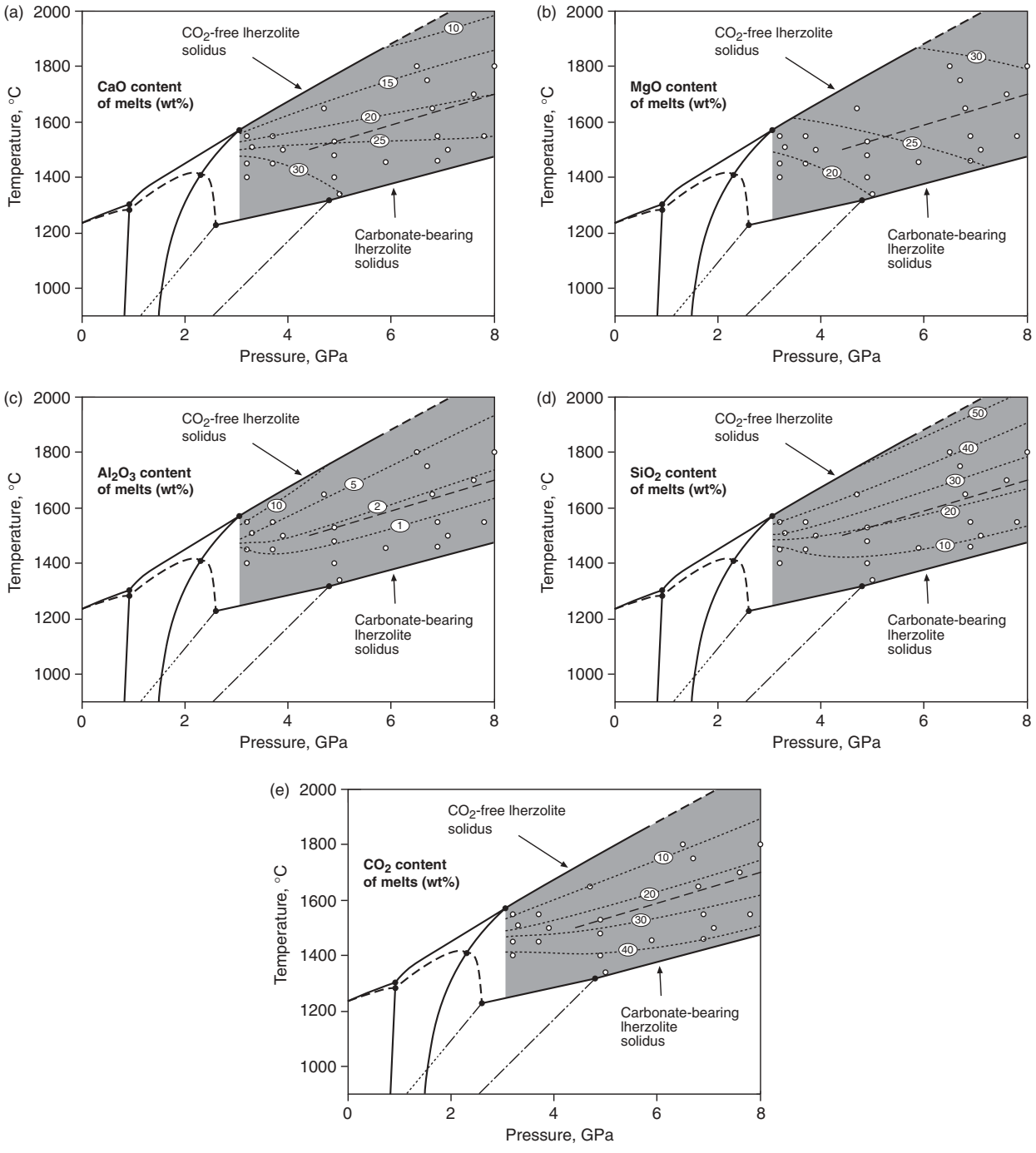

Fig. 4. Isopleths for the oxide contents of melts along the divariant surface involving CO_2-bearing melts in equilibrium with the garnet lherzolite phase assemblage in the CMAS–CO_2 system at 3–8 GPa. The numbers in the ovals indicate per cent oxide content by weight. (a) CaO content; (b) MgO content; (c) Al_2O_3 content; (d) SiO_2 content; (e) CO_2 content.

higher degrees of melting. Compositions resembling group IB kimberlites (Smith *et al.*, 1985) are generated at pressures around 5–6 GPa whereas the compositions of group IA kimberlites (Smith *et al.*, 1985) are consistent with generation at greater depths at pressures around 10 GPa (Fig. 5). The average compositions of kimberlites from Kimberley, South Africa (Clement, 1982) and of Siberian kimberlites (Ilupin & Lutz, 1971) are also consistent with generation in the 5–10 GPa pressure range. Representative compositions of contamination-free kimberlites (Mitchell, 1986) are shown in Fig. 5 for comparison with the experimental data. Although the large

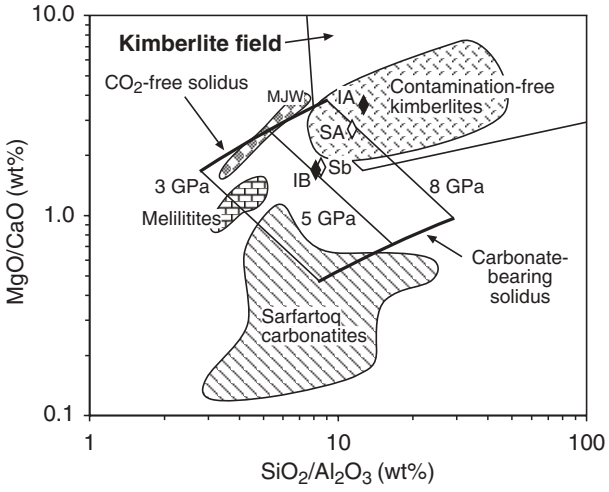

Fig. 5. Compositions of melts generated in equilibrium with garnet lherzolite in the CMAS–CO_2 system shown in a discrimination diagram of MgO/CaO vs SiO_2/Al_2O_3 (wt % ratios) for kimberlites and ultramafic lamprophyres (Rock, 1991). The field for ultramafic lamprophyres, which is outside the kimberlite field, is not relevant to this study and has not been labeled. For clarity, only three isobars (3, 5, and 8 GPa) are shown. The area between the CO_2-free and carbonate-bearing solidi corresponds to the shaded area in Fig. 1. The field for carbonatites from the Sarfartoq region in west Greenland is based on the unpublished data of L. M. Larsen (2003). The average compositions of IA and IB kimberlites are from Smith *et al.* (1985). SA and Sb are the average compositions of kimberlites from Kimberley, South Africa (Clement, 1982) and Siberian kimberlites (Ilupin & Lutz, 1971), respectively. The fields of melilitites and contamination-free kimberlites are based on whole-rock data from Mitchell (1996) and Mitchell (1986), respectively. The field labeled MJW is the compositions of melts generated in equilibrium with the garnet lherzolite phase assemblage at 3–7 GPa in experiments with the volatile-free, natural peridotite KR4003 as starting material (Walter, 1998).

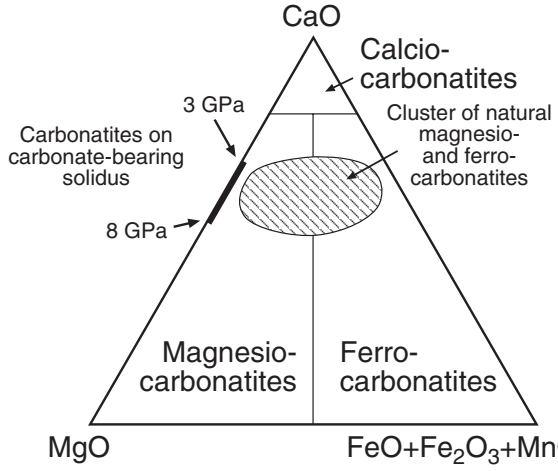

Fig. 6. Comparison of compositions of carbonatitic melts produced along the carbonate-bearing solidus in the CMAS–CO_2 system (Dalton & Presnall, 1998*a*) with the compositions of naturally occurring magnesio- and ferrocarbonatites (Woolley & Kempe, 1989). This classification scheme for carbonatites is from Woolley & Kempe (1989).

compositional spread of these kimberlite whole-rock compositions allows only a rough comparison with our experimental melts, the compositional range of the contamination-free kimberlites suggests that some kimberlites could be generated at still higher pressures, significantly beyond the range of the experimental data (>8 GPa). Thus, as expected, the compositions of kimberlites are consistent with generation at pressures of about 5 GPa or higher, whereas the compositions of melilitites (Mitchell, 1996) are consistent with generation at lower pressures around 3 GPa with less CO_2 in the melt than carbonatites, in good agreement with our experimental results (Fig. 5). Brey (1978) and Canil & Scarfe (1990) have similarly proposed that kimberlites and melilitites differ in their depth of generation in the upper mantle.

Comparison with proposed carbonatitic and kimberlitic primary melt compositions

The nature of primary kimberlite melts has long been a contentious subject. Kimberlite glasses are never found in nature and it is difficult to identify rocks that unambiguously represent kimberlite melts. A few examples of aphanitic kimberlites that retain considerable amounts of CO_2 have been proposed as possibly having compositions close to primitive kimberlite melts. These include kimberlites from the Wesselton mine, South Africa (Shee, 1986; Edgar *et al.*, 1988; Edgar & Charbonneau, 1993) and the Jericho pipe, Canada (Price *et al.*, 2000). In Figs 7–9 the compositions of these possible primitive kimberlite melts have been plotted along with melt compositions from this study in equilibrium with the garnet lherzolite mineral assemblage. If one assumes that the natural compositions are near-primary melts, the Wesselton aphanitic kimberlite is consistent with derivation from a pressure of about 5–8 GPa. The position of the Jericho aphanitic kimberlites on these diagrams is also consistent with the conclusion of Price *et al.* (2000) that the primary melts for these rocks were generated at a pressure of about 6 GPa or slightly higher. In Figs 7 and 8, the Jericho aphanitic kimberlites form a trend that appears consistent with olivine control. However, Fig. 9 shows that SiO_2/Al_2O_3 is very similar in all the samples, but increases slightly with decreasing MgO/CaO, contrary to what one would expect for an olivine control line. Therefore, we suggest that the compositional variation is controlled by the addition and/or removal of calcite phenocrysts in the parental magmas or, alternatively, uncertainty in the relative proportions of silicates and calcite in the analyzed samples.

Van Achterbergh *et al.* (2002) described inclusions in diopside macrocrysts in kimberlite in the Lac de Gras area in Canada that have carbonatite composition. The generation of the alleged carbonatite melts may have

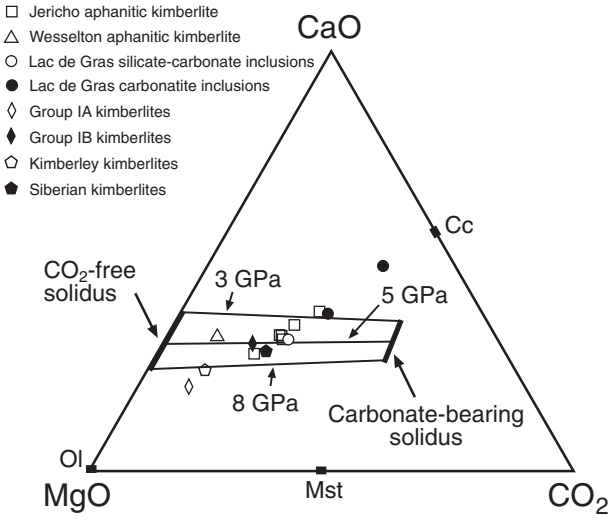

Fig. 7. Compositions of aphanitic kimberlites from the Jericho pipe, Canada (localities JD61 and JD82) (Price *et al.*, 2000) and Wesselton, South Africa (Shee, 1986), and carbonatitic (van Achterbergh *et al.*, 2002) and silicate–carbonate (van Achterbergh *et al.*, 2004) inclusions from the A154N kimberlite in the Lac de Gras area, Canada, in comparison with melts generated in equilibrium with garnet lherzolite in the CMAS–CO_2 system and average Group IA and IB kimberlite compositions (see the caption for Fig. 5 for references). The compositions of olivine (Ol), calcite (Cc), and magnesite (Mst) are also shown.

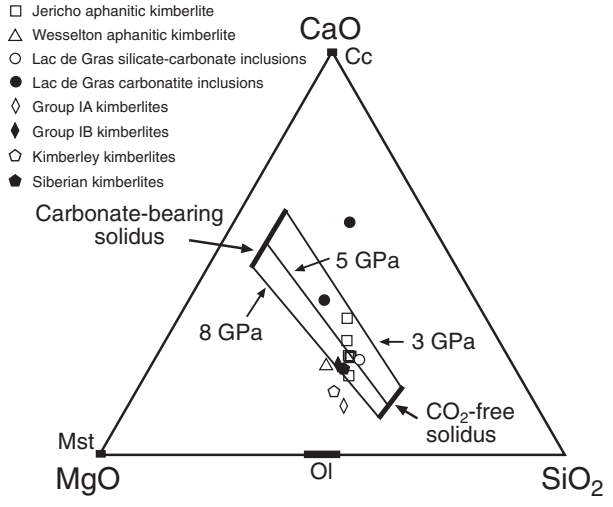

Fig. 8. Compositions of aphanitic kimberlites from the Jericho pipe, Canada (localities JD61 and JD82) (Price *et al.*, 2000) and Wesselton, South Africa (Shee, 1986), and carbonatitic (van Achterbergh *et al.*, 2002) and silicate–carbonate (van Achterbergh *et al.*, 2004) inclusions from the A154N kimberlite in the Lac de Gras area, Canada, in comparison with melts generated in equilibrium with garnet lherzolite in the CMAS–CO_2 system and average Group IA and IB kimberlite compositions (see the caption for Fig. 3 for references). The compositions of olivine (Ol), calcite (Cc), and magnesite (Mst) are also shown. The compositional range of olivine (Ol) is from Fo_{95} to Fo_{70}.

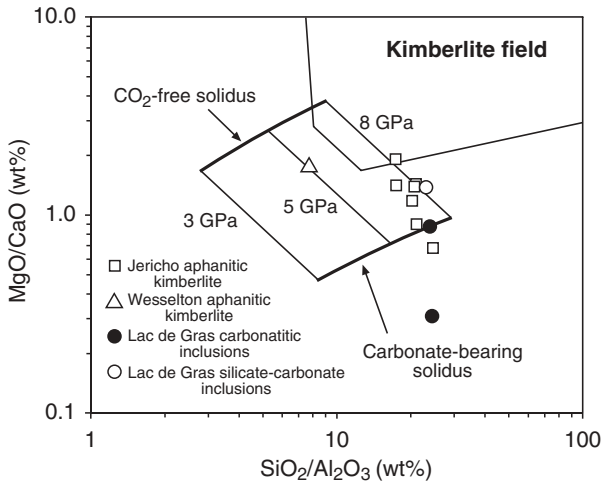

Fig. 9. Discrimination diagram for kimberlites and ultramafic lamprophyre (Rock, 1991) showing compositions of aphanitic kimberlites from Jericho pipe, Canada (localities JD69 and JD82) (Price *et al.*, 2000) and Wesselton mine, Kimberley, South Africa (Shee, 1986), and carbonatitic (van Achterbergh *et al.*, 2002) and silicate–carbonate (van Achterbergh *et al.*, 2004) inclusions from the A154N kimberlite in the Lac de Gras area, Canada, in comparison with melts generated in equilibrium with garnet lherzolite in the CMAS–CO_2 system.

been temporally linked to the kimberlite eruption. Considering the challenge of analyzing the assemblage of microscopic minerals and the potential for fractionation, the compositions of the carbonatite inclusions bear surprisingly strong resemblance to melts generated in the 3–8 GPa pressure range close to the boundary between carbonatites and kimberlites in the CMAS–CO_2 system (Figs 7–9). In a later paper, van Achterbergh *et al.* (2004) described ultramafic silicate–carbonate inclusions from the same kimberlite that they interpreted as unmixed kimberlite melts. It should be noted that, as expected, the inclusions have very small amounts of Al_2O_3 ($\leq$1·3 wt %), which means that SiO_2/Al_2O_3 in Fig. 9 is sensitive to relatively small uncertainties in Al_2O_3. Interestingly, there are strong similarities between the compositions of the carbonatite inclusions and the Jericho aphanitic kimberlites, a further indication of a gradation between kimberlite and carbonatite melts in the mantle.

MELTING PATHS

Our experiments do not answer the question of how much CO_2 there is in the source regime of carbonatites, kimberlites and melilitites, and our results do not preclude the possibility that these source regions have very large amounts of CO_2, such as by earlier episodes of migration of CO_2-rich fluids or melts. In the CMAS–CO_2 system, the melt composition remains the same as long as the whole garnet lherzolite phase assemblage is present but variations in the amount of CO_2 will affect

the proportions of the phases. Increased amounts of CO_2 in the system cause increases in the proportion of melt, which in turn affect the relative proportions of the crystalline phases. Because of the insignificant solubility of carbon in the garnet lherzolite phases (Keppler *et al.*, 2003), CO_2 can be treated as a perfectly incompatible component during melting. Then, with a given bulk amount of CO_2 in a carbonated garnet lherzolite composition in the CMAS–CO_2 system, one can calculate melting contours on the divariant surface on the assumption that all the CO_2 is present in the melt phase. Another inherent assumption is that the garnet lherzolite assemblage is present along the entire melting interval without exhaustion of any phase. As shown below, the generation of kimberlite and carbonatite magmas involves such small degree of melting that this is likely to be the case even with elevated amounts of CO_2 present. Figure 10a and b shows melting contours for garnet lherzolite with a relatively high (1500 ppm) and low bulk CO_2 content (200 ppm), respectively. As required, the contours follow the isopleths for CO_2 in the melt (Fig. 4e). To demonstrate melting paths along the divariant surface, we also show two different adiabats with a potential temperature of 1310°C and 1510°C (labeled A and B, respectively) and a slope of 13 K/GPa (Katsura *et al.*, 2004).

An analysis of published experimental data on the solidi of volatile-free and CO_2-bearing natural peridotite compositions indicates that they could be about 60°C and 200°C lower, respectively, than the comparable solidi in the CMAS–CO_2 and CMAS systems, and the pressure at the edge of the ledge is lowered to about 1·9 GPa (Presnall & Gudfinnsson, 2005). Therefore, the carbonate-bearing and CO_2-free solidi for the simplified system, shown in Fig. 10, are about 200°C and 60°C higher, respectively, than they would be in the mantle (Presnall *et al.*, 2002). With this adjustment, the phase relations shown can be used as a close approximation of phase relations in the mantle. Let us consider, for example, melting of magnesite-bearing mantle material that upwells along adiabat A in Fig. 10a. This relatively cool adiabat intersects the solidus at about 7 GPa at a temperature about 500°C lower than that of the volatile-free solidus. The melting path follows the carbonate-bearing solidus for a very narrow pressure interval until magnesite is exhausted, at which point it enters the divariant surface. Even for a carbon-rich mantle with 0·15 wt % CO_2, this will happen after only about 0·35% melting. Because of the small amount of liquid being generated, an isentropic melting path follows a solid adiabat very closely. The melt composition is magnesiocarbonatite with slightly increasing silica content and decreasing CO_2 content as pressure decreases, and at about 5 GPa the CO_2 content of the melt is about 40 wt % and the amount of melting is nearly 0·4%.

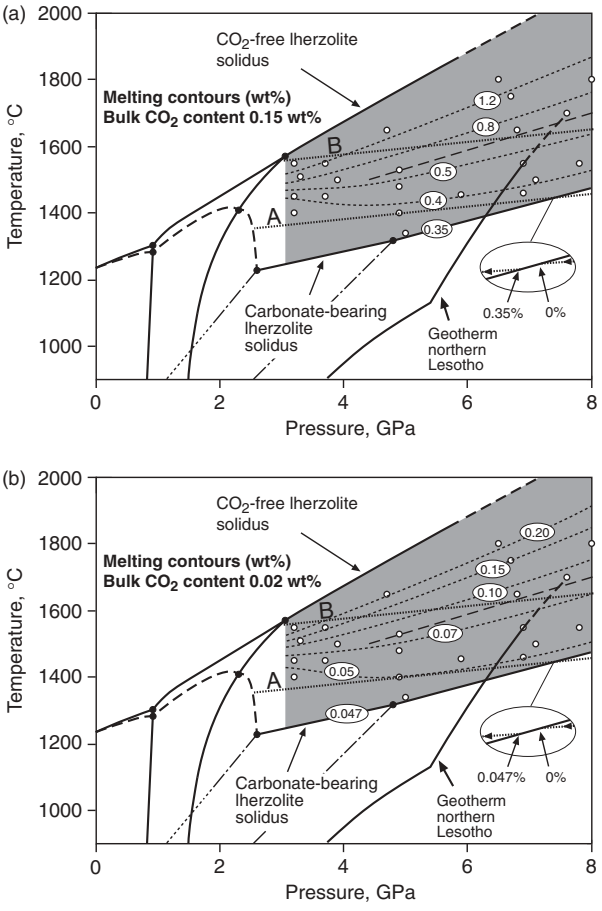

Fig. 10. Pressure–temperature diagram for the solidus of plagioclase, spinel and garnet lherzolite in the CMAS–CO_2 system under CO_2-free and CO_2-bearing conditions. The dotted lines marked A and B are adiabats discussed in the text with a slope of 13 K/GPa and potential temperatures of 1310°C and 1510°C, respectively. The continuous curve on the lower right is the geotherm for northern Lesotho determined by Finnerty & Boyd (1987). The contours on the divariant surface indicate the amount of melting when the bulk CO_2 content is (a) 0·15 wt % and (b) 0·02 wt %. The numbers in ovals indicate the amount of melting in wt %. The amount of CO_2 in the melt is almost identical at the carbonate-bearing solidus at all pressures from 3 to 8 GPa. Therefore, the amount of melting is the same at carbonate exhaustion at any pressure in this range at the carbonate-bearing solidus (indicated by the number in an oval on the solidus). The inset on the lower right shows that in detail the melting path follows the carbonate-bearing solidus over a short pressure interval until magnesite is exhausted (after about 0·35% and 0·047% melting when the bulk CO_2 content is 0·15 and 0·02 wt %, respectively). Modified after Presnall *et al.* (2002).

However, because of the upward curvature of the CO_2 isopleths (and hence the melting contours) the amount of melt does not increase, but instead decreases slightly, at lower pressures, and therefore only carbonatitic melt and no kimberlitic melt is generated along this adiabat in the CMAS–CO_2 system. In contrast, with an elevated geotherm, such as adiabat B in Fig. 10, a larger range of compositions results. In this case, melting starts at a

pressure considerably higher than 8 GPa and the melting path leaves the carbonatite field and passes into the kimberlite field at between 6 and 7 GPa. If the total amount of CO_2 in the system is 0·15 wt %, the amount of melt at this point is about 0·6–0·7%. At lower pressures the melt becomes melilititic, and finally, below 3 GPa, picritic. At this point, the extent of melting is likely to be large enough to cause the melting path to deviate considerably from the solid adiabat. With lower bulk CO_2 contents the melting paths are the same and identical melts are produced; however, the degree of melting is lower at comparable pressures along the adiabats (Fig. 10b). However, if the CO_2 content of the source is very high, the amount of melting is also higher and the melting path would start to deviate significantly from a solid adiabat at higher pressures, resulting in different melt compositions at similar pressures.

On the basis of geothermobarometry studies of mantle xenoliths, Finnerty & Boyd (1987) determined the mantle geotherm beneath Lesotho at the time of kimberlite magmatism (Fig. 10), and concluded that the xenoliths came from a pressure of up to 7 GPa. Extrapolation of this geotherm yields temperatures in the kimberlite field at just below 8 GPa, a pressure slightly higher than the maximum Finnerty & Boyd (1987) estimated for the Lesotho xenoliths. Lowering of the adiabat and phase boundaries by 60–200°C so as to correspond to phase boundaries for the compositionally more complex mantle would produce an excellent match with the conclusion of Finnerty & Boyd (1987).

The effect of additional components

Components other than CaO, MgO, Al_2O_3, SiO_2, and CO_2 are all, except FeO and H_2O, in such a low abundance that their effect on the phase relations during the melting of garnet lherzolite is likely to be minor. In spite of its abundance, the effect of FeO on the lherzolite phase relations is also likely to be relatively small (Gudfinnsson & Presnall, 2000). The effects of FeO and Na_2O on the stability of the carbonates and, by implication, the carbonate-bearing solidus, are more uncertain. On the basis of volatile-bearing experiments, Mysen & Boettcher (1975) proposed kimberlite generation by melting of peridotite at pressures of 4–6 GPa with significant amounts of both CO_2 and H_2O present. Results of experiments on the melting of lherzolite indicate that the effect of modest amounts of water on the phase relations is small (Gaetani & Grove, 1998) and likely to be greatly subordinate to the effect of CO_2. In contrast, the effect of water on the melting temperature could be considerable (Gaetani & Grove, 1998). So far, there have been no studies on the combined effect of water and CO_2 on the solidus of peridotite in the pressure range of interest that include information on the amount of CO_2 and water in the melt. However, the data of Falloon & Green (1990) at 3·5 GPa indicate that the water-saturated solidus of carbonate-bearing peridotite could be up to 150°C lower than the anhydrous solidus. In this case, there were no hydrous crystalline phases present but the presence of such phases could limit the amount of temperature depression at low degrees of melting. The aphanitic kimberlites from the Jericho pipe contain about 5–7 wt % H_2O, which is thought to represent the primary water content of the kimberlites (Price *et al.*, 2000), and carbonatites could carry comparable amounts of water (Le Bas, 1981). Hence, the amount of water present in natural kimberlite and carbonatite magmas indicates that they could be produced at temperatures significantly lower than comparable melts in the CMAS–CO_2 system. Kimberlite melts could then possibly be produced by melting of upwelling CO_2-bearing garnet lherzolite under conditions where the adiabat is not much hotter than an average MORB mantle adiabat of about 1300°C, depending on the water content. As a corollary, carbonatite and kimberlite melt generation may be pervasive at depth wherever the mantle upwells. Because these kinds of melts easily become mobile (Minarik & Watson, 1995; Faul, 2001) and carry very high concentrations of incompatible elements, this could have an important effect on the trace element signatures of basalts when the CO_2-rich melts mix with primitive basalt melts generated at shallower depth (Presnall *et al.*, 2002).

CONCLUSIONS

At pressures from 3 to 8 GPa in the CMAS–CO_2 system, CO_2-bearing melts in equilibrium with the garnet lherzolite phase assemblage show continuous change from magnesiocarbonatites with up to 40–45% CO_2, at the low-temperature side, through kimberlitic and melilititic compositions to komatiites or picritic basalts, at the high-temperature side where the CO_2 content is low. The magnesiocarbonatites have $CaO/(CaO + MgO) = 0·5$–$0·7$, similar to the $CaO/(CaO + MgO + FeO + Fe_2O_3 + MnO)$ of naturally occurring ferro- and magnesiocarbonatites, suggesting that the latter form by very low degree melting in a similar pressure range. The melilitite melts, which are produced only at pressures <4 GPa, resemble natural melilitite whole-rock compositions but grade into kimberlitic melts at higher pressures and temperatures. This indicates that kimberlite genesis requires elevated geotherms relative to those of MORB. However, the amount of water found in some kimberlites and carbonatites lowers the estimated equilibrium temperature, perhaps as much as 150°C. The average compositions of IB and IA kimberlites are consistent with generation at pressures of 5–6 GPa and about 10 GPa, respectively. Some other kimberlite compositions suggest an origin at

even higher pressures. Modeling of the melting of the garnet lherzolite phase assemblage containing 0·15 wt % CO_2 indicates that carbonatites are produced by <0·5% melting and kimberlites and melilitites by <1% melting. Low-degree, CO_2-rich mantle melts could potentially be an important source of incompatible trace elements and control the signature of certain trace elements in basaltic magmas generated at lower pressures.

ACKNOWLEDGEMENTS

We thank Bob Luth and Steve Parman for their highly constructive reviews, and Marjorie Wilson for editorial handling. Lotte Melchior Larsen generously allowed the use of an unpublished set of carbonatite compositions from the Sarfartoq region in west Greenland. Peter Roeder and an anonymous reviewer provided useful comments on an earlier version of this paper. This material is based upon work supported by the National Science Foundation under Grant No. 0106645.

REFERENCES

Bailey, D. K. (1993). Carbonate magmas. *Journal of the Geological Society, London* **150**, 637–651.

Barker, D. S. (1989). Field relations of carbonatites. In: Bell, K. (ed.) *Carbonatites: Genesis and Evolution*. London: Unwin Hyman, pp. 38–69.

Bohlen, S. R. & Boettcher, A. L. (1982). The quartz + coesite transformation: a precise determination and the effects of other components. *Journal of Geophysical Research* **87**, 7073–7078.

Brey, G. (1978). Origin of olivine melilitites—chemical and experimental constraints. *Journal of Volcanology and Geothermal Research* **3**, 61–88.

Brey, G. & Green, D. H. (1977). Systematic study of liquidus phase relations in olivine melilitite + H_2O + CO_2 at high pressures and petrogenesis of an olivine melilitite magma. *Contributions to Mineralogy and Petrology* **61**, 141–162.

Canil, D. & Scarfe, C. M. (1990). Phase relations in peridotite + CO_2 systems to 12 GPa: implications for the origin of kimberlite and carbonate stability in the Earth's upper mantle. *Journal of Geophysical Research* **95**, 15805–15816.

Clement, C. R. (1982). A comparative geological study of some major kimberlite pipes in the northern Cape and Orange Free State. Ph.D. thesis, University of Cape Town.

Dalton, J. A. & Presnall, D. C. (1998*a*). Carbonatitic melts along the solidus of model lherzolite in the system CaO–MgO–Al_2O_3–SiO_2–CO_2 from 3 to 7 GPa. *Contributions to Mineralogy and Petrology* **131**, 123–135.

Dalton, J. A. & Presnall, D. C. (1998*b*). The continuum of primary carbonatitic–kimberlitic melt compositions in equilibrium with lherzolite: data from the system CaO–MgO–Al_2O_3–SiO_2–CO_2 at 6 GPa. *Journal of Petrology* **39**, 1953–1964.

Edgar, A. D. & Charbonneau, H. E. (1993). Melting experiments on a SiO_2-poor, CaO-rich aphanitic kimberlite from 5–10 GPa and their bearing on sources of kimberlite magmas. *American Mineralogist* **78**, 132–142.

Edgar, A. D., Arima, M., Baldwin, D. K., Bell, D. R., Shee, S. R., Skinner, E. M. W. & Walker, E. C. (1988). High-pressure–high-temperature melting experiments on a SiO_2-poor aphanitic kimberlite from the Wesselton mine, Kimberley, South Africa. *American Mineralogist* **73**, 524–533.

Eggler, D. H. (1976). Does CO_2 cause partial melting in the low-velocity layer of the mantle? *Geology* **4**, 69–72.

Falloon, T. J. & Green, D. H. (1990). Solidus of carbonated fertile peridotite under fluid-saturated conditions. *Geology* **18**, 195–199.

Faul, U. H. (2001). Melt retention and segregation beneath mid-ocean ridges. *Nature* **410**, 920–923.

Finnerty, A. A. & Boyd, F. R. (1987). Thermobarometry for garnet peridotites: basis for the determination of thermal and compositional structure of the upper mantle. In: Nixon, P. H. (ed.) *Mantle Xenoliths*. Chichester: John Wiley, pp. 381–402.

Gaetani, G. A. & Grove, T. L. (1998). The influence of water on melting of mantle peridotite. *Contributions to Mineralogy and Petrology* **131**, 323–346.

Gudfinnsson, G. H. & Presnall, D. C. (1996). Melting relations of model lherzolite in the system CaO–MgO–Al_2O_3–SiO_2 at 2·4–3·4 GPa and the generation of komatiites. *Journal of Geophysical Research* **101**, 27701–27709.

Gudfinnsson, G. H. & Presnall, D. C. (2000). Melting behaviour of model lherzolite in the system CaO–MgO–Al_2O_3–SiO_2–FeO at 0·7–2·8 GPa. *Journal of Petrology* **41**, 1241–1269.

Harmer, R. E. & Gittins, J. (1998). The case for primary, mantle-derived carbonatite magma. *Journal of Petrology* **39**, 1895–1903.

Ilupin, I. P. & Lutz, B. G. (1971). The chemical composition of kimberlite and questions on the origin of kimberlite magmas. *Sovetskaya Geologiya* **6**, 61–73 (in Russian).

Irving, A. J. & Wyllie, P. J. (1975). Subsolidus and melting relationships for calcite, magnesite and the join $CaCO_3$–$MgCO_3$ to 36 kb. *Geochimica et Cosmochimica Acta* **39**, 35–53.

Katsura, T., Yamada, H., Nishikawa, O., Song, M., Kubo, A., Shinmei, T., Yokoshi, S., Aizawa, Y., Yoshino, T., Walter, M. J., Ito, E. & Funakoshi, K. (2004). Olivine–wadsleyite transition in the system $(Mg,Fe)_2SiO_4$. *Journal of Geophysical Research* **109**, B02209, doi:10.1029/2003JB002438.

Keppler, H., Wiedenbeck, M. & Shcheka, S. S. (2003). Carbon solubility in olivine and the mode of carbon storage in the Earth's mantle. *Nature* **424**, 414–416.

Le Bas, M. J. (1981). Carbonatite magmas. *Mineralogical Magazine* **44**, 133–140.

Milholland, C. S. & Presnall, D. C. (1998). Liquidus phase relations in the CaO–MgO–Al_2O_3–SiO_2 system at 3·0 GPa: the aluminous pyroxene thermal divide and high-pressure fractionation of picritic and komatiitic magmas. *Journal of Petrology* **39**, 3–27.

Minarik, W. G. & Watson, E. B. (1995). Interconnectivity of carbonate melt at low melt fraction. *Earth and Planetary Science Letters* **133**, 423–437.

Mitchell, R. H. (1986). *Kimberlites: Mineralogy, Geochemistry, and Petrology*. New York: Plenum.

Mitchell, R. H. (1995). *Kimberlites, Orangeites, and Related Rocks*. New York: Plenum.

Mitchell, R. H. (1996). The melilitite clan. In: Mitchell, R. H. (ed.) *Undersaturated Alkaline Rocks: Mineralogy, Petrogenesis, and Economic Potential. Mineralogical Association of Canada, Short Course Series* **24**, 123–151.

Moore, K. R. & Wood, B. J. (1998). The transition from carbonate to silicate melts in the CaO–MgO–SiO_2–CO_2 system. *Journal of Petrology* **39**, 1943–1951.

Mysen, B. & Boettcher, A. L. (1975). Melting of a hydrous mantle: I. Phase relations of natural peridotite at high pressures and temperatures with controlled activities of water, carbon dioxide, and hydrogen. *Journal of Petrology* **16**, 520–548.

Nelson, D. R., Chivas, A. R., Chappell, B. W. & McCulloch, M. T. (1988). Geochemical and isotopic systematics in carbonatites and

implications for the evolution of ocean-island sources. *Geochimica et Cosmochimica Acta* **52**, 1–17.

Presnall, D. C. (1986). An algebraic method for determining equilibrium crystallization and fusion paths in multicomponent systems. *American Mineralogist* **71**, 1061–1070.

Presnall, D. C. & Gudfinnsson, G. H. (2005). Carbonate-rich melts in the oceanic low-velocity zone and deep mantle. In: Foulger, G. R., Natland, J. H., Presnall, D. C. & Anderson, D. L. (eds) *Plates, Plumes and Paradigms. Geological Society of America, Special Papers* **388** (in press).

Presnall, D. C., Gudfinnsson, G. H. & Walter, M. J. (2002). Generation of mid-ocean ridge basalts at pressures from 1 to 7 GPa. *Geochimica et Cosmochimica Acta* **66**, 2073–2090.

Price, S. E., Russell, J. K. & Kopylova, M. G. (2000). Primitive magma from the Jericho pipe, N.W.T., Canada: constraints on primary kimberlite melt chemistry. *Journal of Petrology* **41**, 789–808.

Rock, N. M. S. (1991). *Lamprophyres*. Glasgow: Blackie.

Shee, S. R. (1986). The petrogenesis of the Wesselton mica kimberlites, Kimberley, South Africa. Ph.D. thesis, University of Cape Town.

Smith, C. B., Gurney, J. J., Skinner, E. M. W., Clement, C. R. & Ebrahim, N. (1985). Geochemical character of southern African kimberlites: a new approach based on isotopic constraints. *Transactions of the Geological Society of South Africa* **88**, 267–280.

Susaki, J., Akaogi, M., Akimoto, S. & Shimomura, O. (1985). Garnet–perovskite transformation in $CaGeO_3$: *in-situ* X-ray measurements using synchrotron radiation. *Geophysical Research Letters* **12**, 729–732.

Van Achterbergh, E., Griffin, W. L., Ryan, C. G., O'Reilly, S. Y., Pearson, N. J., Kivi, K. & Doyle, B. J. (2002). Subduction signature for quenched carbonatites from the deep lithosphere. *Geology* **30**, 743–746.

Van Achterbergh, E., Griffin, W. L., Ryan, C. G., O'Reilly, S. Y., Pearson, N. J., Kivi, K. & Doyle, B. J. (2004). Melt inclusions from the deep Slave lithosphere: implications for the origin and evolution of mantle-derived carbonatite and kimberlite. *Lithos* **76**, 461–474.

Walter, M. J. (1998). Melting of garnet peridotite and the origin of komatiite and depleted lithosphere. *Journal of Petrology* **39**, 29–60.

Weng, Y.-H. (1997). Liquidus phase relations for the model basaltic tetrahedron diopside–anorthite–forsterite–quartz in the system CaO–MgO–Al_2O_3–SiO_2 at 5 GPa. Ph.D. dissertation, University of Texas at Dallas, 76 pp.

Woolley, A. R. & Kempe, D. R. C. (1989). Carbonatites: nomenclature, average chemical compositions, and element distribution. In: Bell, K. (ed.) *Carbonatites: Genesis and Evolution*. London: Unwin Hyman, pp. 1–14.

Woolley, A. R., Bergman, S. C., Edgar, A. D., Le Bas, M. J., Mitchell, R. H., Rock, N. M. S. & Scott Smith, B. H. (1996). Classification of lamprophyres, lamproites, kimberlites, and the kalsilitic, melilitic, and leucitic rocks. *Canadian Mineralogist* **34**, 175–186.

Wyllie, P. J. & Huang, W.-L. (1975). Influence of mantle CO_2 in the generation of carbonatites and kimberlites. *Nature* **257**, 297–299.